BMC Medicine

RESEARCH

Open Access

Bridging animal models and humans: neuroimaging as intermediate phenotypes linking genetic or stress factors to anhedonia

Huiling Guo[1,2†], Yao Xiao[1†], Shuai Dong[1,2], Jingyu Yang[1], Pengfei Zhao[1], Tongtong Zhao[1], Aoling Cai[1,2,3], Lili Tang[1], Juan Liu[1], Hui Wang[4], Ruifang Hua[4], Rongxun Liu[1,4], Yange Wei[1,4], Dandan Sun[5], Zhongchun Liu[6,7], Mingrui Xia[8,9,10], Yong He[8,9,10,11], Yankun Wu[12], Tianmei Si[12], Fay Y. Womer[13], Fuqiang Xu[14,15,16,17], Yanqing Tang[18], Jie Wang[19*], Weixiong Zhang[20*], Xizhe Zhang[1,2*] and Fei Wang[1,21*]

Abstract

Background Intermediate phenotypes, such as characteristic neuroimaging patterns, offer unique insights into the genetic and stress-related underpinnings of neuropsychiatric disorders like depression. This study aimed to identify neuroimaging intermediate phenotypes associated with depression, bridging etiological factors to behavioral manifestations and connecting insights from animal models to diverse clinical populations.

Methods We analyzed datasets from both rodents and humans. The rodent studies included a genetic model (P11 knockout) and an environmental stress model (chronic unpredictable mild stress), while the human data comprised 748 participants from three cohorts. Using the amplitude of low-frequency fluctuations, we identified neuroimaging patterns in rodent models. We then applied a machine-learning approach to cluster neuroimaging subtypes of depression. To assess the genetic predispositions and stress-related changes associated with these subtypes, we analyzed genotype and metabolite data. Linear regression was employed to determine which neuroimaging features predicted core depression symptoms across species.

Results The genetic and environmental stress models exhibited distinct neuroimaging patterns in subcortical and sensorimotor regions. Consistent patterns emerged in two neuroimaging subtypes identified across three independent depressed cohorts. The subtype resembling P11 knockout demonstrated higher genetic susceptibility, with enriched expression of risk genes in brain tissues and abnormal metabolites linked to tryptophan metabolism. In contrast, the stress animal-like subtype did not show changes in genetic risk scores but exhibited enriched risk gene expression in somatic and endocrine tissues, along with mitochondrial dysfunction in the antioxidant stress system.

†Huiling Guo and Yao Xiao contributed equally to this work.

*Correspondence:
Jie Wang
jie.wang@wipm.ac.cn
Weixiong Zhang
weixiong.zhang@polyu.edu.hk
Xizhe Zhang
zhangxizhe@njmu.edu.cn
Fei Wang
fei.wang@yale.edu
Full list of author information is available at the end of the article

Notably, these distinct subcortical-sensorimotor neuroimaging patterns predicted anhedonia, a core symptom of depression, in both rodent models and depressed subtypes.

Conclusions This cross-species validation suggests that these neuroimaging patterns may serve as robust intermediate phenotypes, linking etiology to anhedonia and facilitating the translation of findings from animal models to humans with depression and other psychiatric disorders.

Keywords Depression, Subtypes, Animal, Neuroimaging, Intermediate phenotypes, Cross-species

Background

Depression is a highly heterogeneous disorder influenced by various genetic and environmental stressors, resulting in variability in symptoms, progression, and treatment response [1]. While animal models have been instrumental in capturing aspects of the complex etiology and pathophysiology of depression, substantial gaps remain in the translational application of animal neuroscience to depression research [2, 3]. Conventional animal models bridge to human depression based on certain shared behaviors, typically capturing only limited aspects of its etiology [4]. The multifactorial etiopathogenesis of depression, along with the unique aspects of human biology, makes it impossible for any single animal model to fully recapitulate the phenotypic spectrum of the disorder [5]. For instance, anhedonia, a core symptom of depression [6], has been simulated in rodent models through different etiological approaches, such as genetic alterations [e.g., P11 knockout mice (P11 KO)] [7] and stress conditioning (e.g., chronic unpredictable mild stress (CUMS) in rodents) [8]. However, the neural mechanisms underlying anhedonia-like behaviors in these distinct rodent models, and their relevance to human depression, remain unclear. Investigating neural intermediate phenotypes that link behavioral manifestations with the differential influences of genes and stress may enhance our understanding of the pathogenesis of depression and improve the translational application of animal models in the complex landscape of human depression research [9].

Objective neurobiological measurements, such as resting-state functional magnetic resonance imaging (fMRI), have been utilized to identify neural subtypes of depression and investigate their neurobiological basis and clinical characteristics [10, 11]. For instance, Drysdale et al. successfully identified four depression subtypes characterized by distinct frontostriatal and limbic functional connectivity patterns in males and females aged 18–65 [12]. Previous research, involving participants aged 13–45 and encompassing both sexes, revealed shared structural and functional deficits in higher-order brain regions and primary cortices among depression, schizophrenia, and bipolar disorder [13, 14]. Several subsequent studies identified two subtypes across these disorders with distinct patterns in the prefrontal cortex, subcortical, and sensorimotor cortices [15, 16]. These subtypes differed in genetic predispositions, as measured by polygenic risk scores, suggesting varying degrees of genetic influence and the potential impact of stress factors [16]. These findings suggest that neuroimaging patterns across higher-order regions and primary cortices may reflect etiological differences in psychiatric disorders, including depression.

However, it remains unknown whether similar neural subtypes exist in rodent models of depression. Establishing such intermediate phenotypes could enhance our understanding of the etiologies of depression and facilitate the translation of findings from animal models to corresponding human depression subtypes based on pathophysiology.

Encouraged by the results of subtyping depression using neuroimaging patterns and guided by our goal of identifying genetic and stress-related animal models to better characterize depression subtypes, we aimed to explore neuroimaging-based intermediate phenotypes that underlie the diverse etiologies of depression. In this framework (Fig. 1), we established etiology-specific animal models of depression to understand brain neuroimaging patterns in genetically and stress-distinct depression subtypes. We then employed an unsupervised machine learning approach to identify and validate neuroimaging subtypes of depression in three independent cohorts. We found common neuroimaging features between these depression subtypes and the etiology-specific animal models. To confirm the biological relevance of the neuroimaging biomarkers, we utilized genotypic and metabolic variations to validate the genetic and stress-related mechanisms associated with the identified subtypes. Furthermore, to demonstrate the utility of neuroimaging intermediate phenotypes in linking to behavioral manifestations, we trained machine learning models to predict behaviors using shared neuroimaging features across both rodent models and human cohorts. This integrated approach allowed us to examine and deconvolute the different etiologies that contribute to the development of depression, identify neuro-biomarkers, and establish links between the complex etiologies and behavioral outcomes.

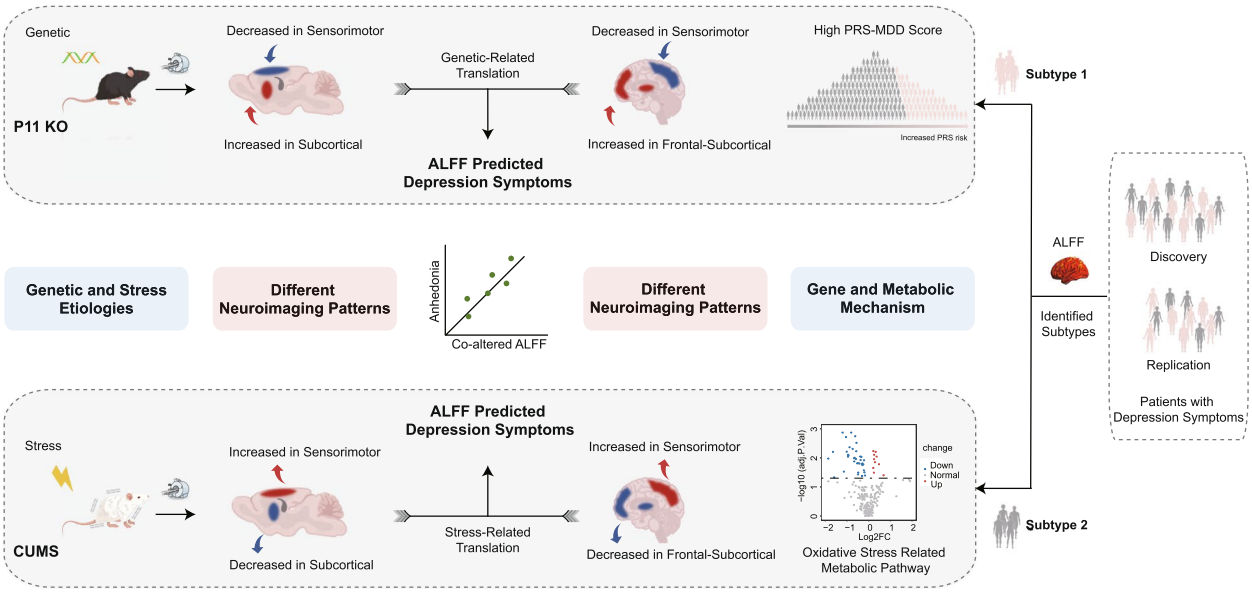

Fig. 1 Overview of the approach to identify rodent models corresponding to depression subtypes based on the concordance of intermediate phenotypes with distinct depression etiologies. To achieve the objectives, we first developed a genetic and environmental stress animal model of depression to identify the ALFF patterns of depression underlying distinct etiology. Next, we constructed a t-SEN and hierarchical cluster approach to define the neuroimaging subtypes of depression and validated cross-species concordance of neuroimaging features, genetic risk score, and metabolic mechanism between etiology-specific animal models and depression subtypes. Finally, we performed linear regression models based on co-altered ALFF values in animals and their corresponding subtypes to predict the core symptoms of depression and investigated the association between neuroimaging and clinical symptoms. ALFF, the amplitude of low-frequency fluctuation; P11 KO, P11 knockout; CUMS, chronic unpredicted mild stress; t-SEN, t-distributed stochastic neighbor embedding; PRS-MDD, polygenetic risk score of major depressive disorder

Methods

Animal study

Animals

P11 KO, a genetic rodent model for depression, and a model of environmental stress (CUMS) were used to investigate the biological mechanisms of depression caused by genetic or stress factors. The study involved 12 wild-type C57BL/6J male mice, 11 P11 KO mice, 15 control rats without CUMS exposure, and 15 male Sprague–Dawley rats undergoing CUMS. A detailed description of the animal model establishment is available in the Methods of Additional file 1 [8, 17]. All procedures in these experiments adhered to the Animal Care and Use Committee guidelines at the Wuhan Institute of Physics and Mathematics, Chinese Academy of Sciences.

Animal behavioral assessments

To assess depression-like behaviors in animals, the following behavioral tests were conducted: the sucrose preference test (SPT) [18], the forced swim test (FST) [19], and the open field test (OFT). Detailed descriptions of these tests are provided in the Methods of Additional file 1.

Animal MRI acquisition

Whole-brain fMRI data were acquired using a gradient-echo echo-planar imaging (GE EPI) sequence to measure the amplitude of low-frequency fluctuations (ALFF) [20]. For detailed scanning sequence parameters and image preprocessing, please refer to the Methods of Additional file 1 [21–23].

Human study

Participants

A total of 748 participants (412 with depression and 336 healthy controls [HC]) were recruited from three independent sites for separate studies. The first cohort was collected at the Renmin Hospital of Wuhan University (WHU: 225 with depression and 65 HC); the second at the Peking University Sixth Hospital (PKU: 75 with depression and 73 HC); and the third at the First Affiliated Hospital of China Medical University (CMU: 112 with depression and 198 HC). Detailed demographic and clinical data of the participants are provided in Additional file 1: Tables S1 and S2. All participants gave written informed consent after receiving a detailed study description. The study was approved by the respective

hospitals' Ethics Committees or Institutional Review Boards.

Clinical assessments

For all participants, symptom measures were obtained using the 17-item Hamilton Depression Rating Scale (HAMD-17) [24] and Snaith-Hamilton Pleasure Scale (SHAPS) [25].

Human MRI acquisition and preprocessing

Functional images were acquired using a GE EPI sequence for ALFF measures. Additionally, functional connectivity (FC) was assessed to analyze alterations in neuroimaging subtypes of depression across different functional imaging modalities. Detailed scanning sequence parameters and image preprocessing steps are provided in the Methods of Additional file 1 [26].

Identifying neuroimaging subtypes in humans

To identify neuroimaging subtypes of depression based on high-dimensional ALFF data, we performed the t-distributed Stochastic Neighbor Embedding (t-SNE) [27] algorithm to reduce the whole brain original high-dimensional ALFF data to two-dimensional representations in depression patients. We then used an agglomerative hierarchical clustering algorithm [28] to cluster the participants into two subtypes. The t-SNE and agglomerative hierarchical clustering algorithms were implemented based on the machine learning library scikit-learn (version 0.22.2.post1) [29]. The consensus clustering algorithm [30] was used to evaluate the stability of the clustering results. To evaluate the diagnostic performance of subtypes, we trained classification models based on 3D residual networks [31] (3D ResNet) to distinguish each subtype from HC, all depression patients from HC, and one subtype from the other subtype. Permutation testing was employed to prove that the subtyping result was not a by-product of the random structure of the dataset.

To assess the robustness of the identified patterns in the WHU cohort, we applied the same clustering method used in the WHU cohort to the PKU cohort (Methods of Additional file 1) [32–35]. Subsequently, we computed the Pearson correlation between the whole-brain *t*-test difference maps of subtypes derived from the WHU and PKU cohorts to analyze the similarity of subtypes across different cohorts. To further evaluate the transferability of the neuroimaging characteristics of the subtypes, we trained a subtype classifier using 3D ResNet on data from the WHU dataset to classify patients of PKU into subtypes. Finally, we compared the subtype labels obtained from clustering and classification methods.

In addition, polygenic risk scores for major depressive disorder (PRS-MDD), risk gene expression, and metabolite data analyses for different subtypes were validated in the CMU cohort. For detailed methods, please refer to the Methods of Additional file 1 [36–40].

Statistical analysis

Animal behavioral

For the depression-like behaviors, two-sample *t*-tests were performed to compare the SPT, FST, and OFT data between wild-type mice and P11 KO, as well as between control rats and the CUMS group. Statistical significance was set at $P < 0.05$.

Animal ALFF

To evaluate ALFF alterations in P11 KO mice and CUMS rats, we performed voxel-based *t*-tests using toolbox for Data Processing and Analysis of Brain Imaging (DPABI) to compare wild-type mice with P11 KO mice and control rats with CUMS rats. Statistical significance was set at voxel $P < 0.05$ and cluster $P < 0.05$, as determined by Gaussian Random Field (GRF) correction.

Depression subtypes clinical assessments

ANOVA was performed to examine demographic and clinical characteristics between the HC and each depression subtype. Statistical significance was set at $P < 0.05$, with Bonferroni correction for multiple comparisons. The chi-square test was used to assess differences in first-episode status between depression subtype 1 and subtype 2, with a significance level set at $P < 0.05$.

Depression subtypes ALFF alterations

To assess the functional deficits in each patient subtype, three-group (HC, subtype 1, and subtype 2) analyses of ALFF and FC values were conducted in DPABI using ANCOVA. The diagnostic group was treated as the independent factor, with age, sex, right-handedness, and education included as covariates in the WHU cohort, and age, sex, medication, and education as covariates in the PKU and CMU cohorts. Statistical significance was set at voxel $P < 0.05$ and cluster $P < 0.05$, as determined by GRF correction. Post hoc analyses were performed to examine the differences between subtype 1, subtype 2, and the HC group. Statistical significance was set at $P < 0.05$.

Depression subtypes multi-level biological validation

Using a *P*-value-informed clumping approach with an R^2 cutoff of 0.1 within a 250-kb window, we derived multiple *P*-value thresholds (PT), including 10^{-8}, 10^{-7}, 10^{-6}, 10^{-5}, 10^{-4}, 10^{-3}, and 0.01, for each set of PRS-MDD. Associations between PRS-MDD and each subtype were evaluated using logistic regression, with

Nagelkerke's pseudo-R^2 calculated to determine the proportion of variance explained.

A total of 270 metabolites were included in the subsequent statistical analysis. Univariate analyses, specifically the nonparametric Mann–Whitney-Wilcoxon test and Benjamini–Hochberg False Discovery Rate (FDR) correction, were used to identify differentially abundant metabolites between subtype 1, subtype 2, and HC. Finally, pathway analyses using Metabo Analyst 5.0 were performed to elucidate disrupted metabolic pathways specific to each subtype. Statistically significant results were defined by P values < 0.05 and FDR < 0.05.

Predicting anhedonia symptoms based on co-altered ALFF patterns

To determine the co-altered characteristics between animal models and corresponding depression subtypes, we defined regions of interest (ROIs) based on standard anatomical templates used in the spatial normalization during preprocessing. ALFF values were then extracted from these ROIs and their subregions. Post hoc analyses were performed to compare wild-type mice with P11 KO, control rats with the CUMS group, and HC with each depression subtype, focusing on co-altered regions using the two-sample t-test. Statistical significance was set at a voxel P value < 0.05.

Stepwise linear regression models were used to examine the relationship between co-altered ROIs and anhedonia by analyzing brain function alterations and behavior. For each animal model or subtype, we calculated the mean ALFF values of each subregion from the co-altered ROIs. A stepwise linear regression model was then trained for each subregion to predict the anhedonia score based on the mean ALFF value of the selected subregions. The Pearson correlation between the predicted and true scale scores was calculated, with the highest correlation being reported. Finally, we identified the combination of voxel ALFF values that best predicted the behavioral scale score in both animal models and depression subtypes. The performance of the regression model was assessed by calculating the Pearson correlation coefficient between the predicted and measured scores. Statistical significance was set at a voxel P value < 0.05.

To illustrate the bridging role of neuroimaging between neural mechanisms and depressive symptoms, we conducted linear regression analyses to identify associations of PRS-MDD or metabolite abnormalities with neuroimaging features and depressive symptoms, followed by mediation analyses. The significance of the coefficients was evaluated using a bias-corrected percentile bootstrap method, with 5000 resamples to estimate 95% confidence intervals for the mediation effect.

Results

Specified patterns of brain function in etiologically distinct rodent models of depression

Animal models typically represent specific aspects of complex diseases such as depression and may be used to represent different etiologic processes in depression. Hence, we examined P11 KO mice as a genetic venue for depression and CUMS rats as an environmental stress pathway to the disorder. Compared to wild-type mice, P11 KO mice had significantly increased ALFF in subcortical regions, including the hippocampus, amygdala, striatum, pallidum, thalamus, and hypothalamus; they also had significantly decreased ALFF in sensorimotor regions, including the primary motor and somatosensory cortices (Fig. 2a, Additional file 1: Table S3). In contrast, compared to non-stressed rat controls, CUMS rats had significantly decreased ALFF in subcortical regions, including the hippocampus, amygdala, striatum, pallidum, and thalamus, and significantly increased ALFF in sensorimotor regions, including the primary motor and somatosensory cortices (Fig. 2a, Additional file 1: Table S4). Interestingly, the ALFF values extracted from significant regions (Additional file 1: Fig S1a and S1b) and the Pearson correlation coefficient between the whole-brain t-test difference maps of these two models ($R = -0.568$, $P_{perm} = 0.011$; Additional file 1:Fig S2) revealed opposing patterns. The converse patterns of functional balance across subcortical and sensorimotor regions may reflect distinctive neural trajectories driven by the different predominance of genetic versus environmental factors between P11 KO and CUMS rodents.

Identification of depression subtypes with different patterns of brain function

To establish a cross-species intermediate phenotype for depression, it is essential to determine whether depressed individuals exhibit similar ALFF patterns to those observed in P11 KO and CUMS rodent models (Fig. 2a). To this end, we first used the t-SNE method and an agglomerative clustering algorithm to delineate two clusters or subtypes in the WHU depressed participants ($N = 225$). Subtype 1 consisted of 56.9% ($N = 128$) of the WHU-depressed cohort, and subtype 2 comprised 43.1% ($N = 97$). No significant difference in age ($F_{(2,287)} = 1.86$, $P = 0.16$) or sex ($\chi^2 = 2.24$, $P = 0.33$) was observed between subtypes and HC ($N = 65$). Demographic and clinical details of the subtypes are in Additional file 1:Table S1.

After delineating the two subtypes in the WHU cohort, we examined ALFF alterations of each subtype compared to HC. Intriguingly, the two subtypes showed distinct ALFF patterns across frontal-subcortical and sensorimotor regions. Specifically, subtype 1 was characterized by significantly elevated ALFF in the frontal-subcortical

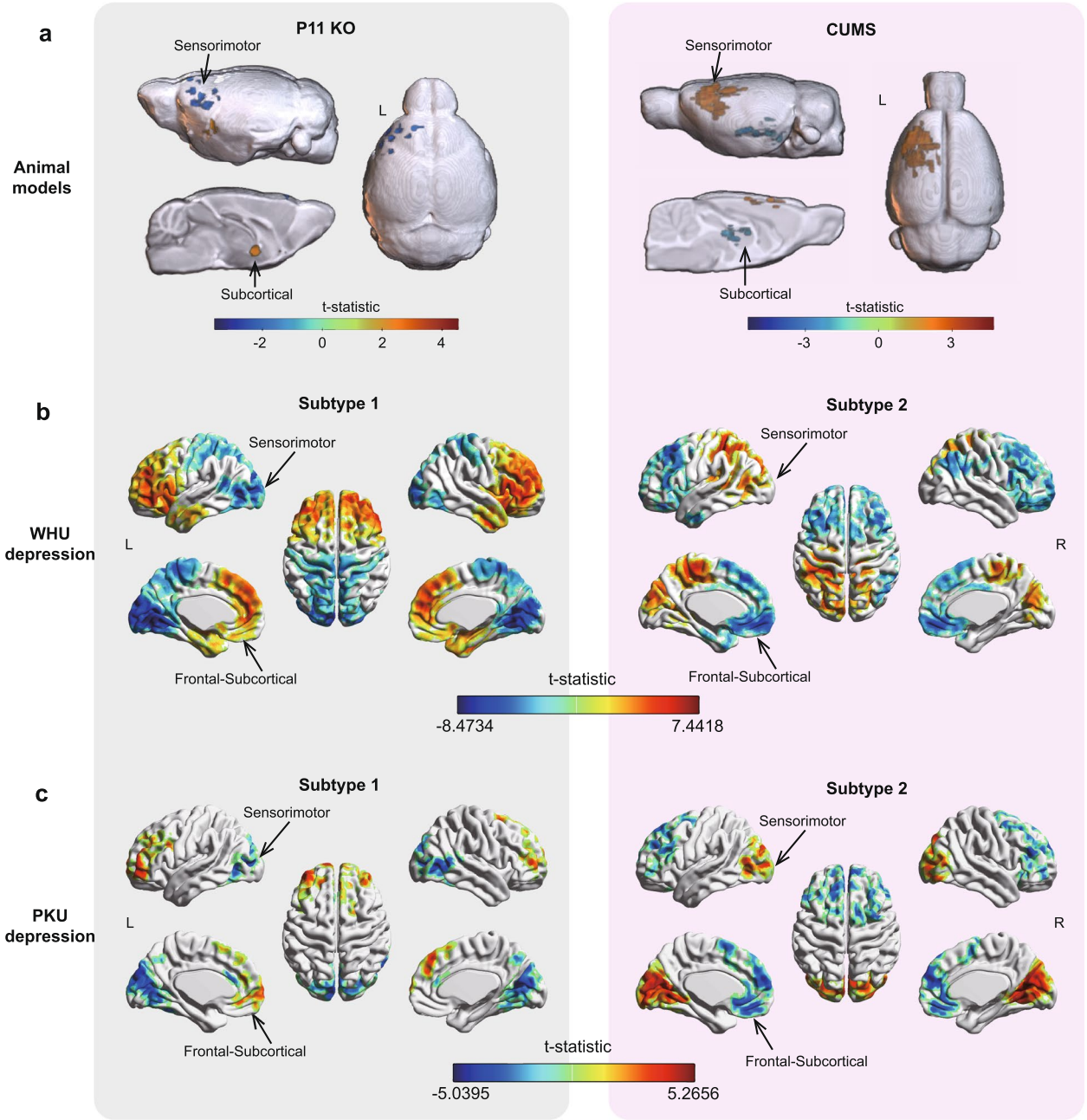

Fig. 2 The etiology-specific animal models and depression subtypes exhibited similar ALFF patterns. **a** The ALFF differences between the P11 KO ($N = 11$) and wild-type mice ($N = 12$) and between CUMS ($N = 15$) and control rats ($N = 15$), assessed in a two-sample *t*-test. The genetic (left, P11 KO mice) and environmental stress (right, CUMS) models exhibited opposite ALFF patterns in subcortical and sensorimotor areas. **b** The ALFF patterns of two depression subtypes compared to HC from the Wuhan cohort ($N = 225$ patients with depression, $N = 65$ healthy control). The altered regions of ALFF of subtype 1 were similar to the P11 KO mice (left); the ALFF patterns of subtype 2 were similar to that of the CUMS (right). **c** The ALFF pattern of subtype 1 and subtype 2 in the PKU cohort ($N = 75$ patients with depression, $N = 73$ healthy control) exhibited similar patterns to that of the Wuhan cohort and animal models. The significance level was set to voxel $P < 0.05$ with Gaussian random field correction for cluster $P < 0.05$. The color bar represents the *t*-statistic values, where warm shades (red) indicate significantly increased ALFF in the animal models or depression subtypes compared to the control group, and cool shades (blue) indicate significantly decreased ALFF. ALFF, the amplitude of low-frequency fluctuation; P11 KO, P11 knockout; CUMS, chronic unpredicted mild stress; WHU, the Renmin Hospital of Wuhan University; PKU, the Peking University Sixth Hospital; L, left; R, right

regions, including the prefrontal cortex, orbital frontal cortex, cingulate, insular, hippocampus, amygdala, striatum and pallidum, and significantly decreased ALFF in the sensorimotor areas, including the primary motor cortex, somatosensory cortex, and visual cortex, compared to HC. Conversely, subtype 2 had significantly decreased ALFF in the frontal-subcortical regions, including the prefrontal cortex, orbital frontal cortex, cingulate, insular, hippocampus, amygdala, striatum, pallidum and thalamus, and significantly increased ALFF in the sensorimotor regions, including the primary motor cortex, somatosensory cortex, and visual cortex, compared to HC (Fig. 2b, Additional file 1: Table S5). Like findings in animal models, the ALFF values extracted from regions showing significant differences (Additional file 1: Fig S1c), along with the Pearson correlation coefficient between the whole-brain t-test difference maps of these two subtypes compared to HC ($R = -0.849$, $P_{perm} < 0.001$; Additional file 1:Fig S3), demonstrate that these subtypes exhibit contrasting abnormal changes. Additionally, these subtypes exhibited contrasting FC patterns between the frontal and primary cortex (Additional file 1: Fig S4). The convergence of results between ALFF and FC analyses supports the robustness of our identified subtypes and reinforces the consistency of our findings across different neuroimaging metrics. Importantly, diagnostic and classification performance demonstrates that the ALFF-based subtypes exhibit high stability and improved diagnostic accuracy for depression (Additional file 1: Fig S5 and S6).

To validate the reproducibility of our subtype findings, we performed a parallel analysis on an independent cohort from PKU, consisting of 75 patients with depression. Using the same feature selection process as in the WHU cohort, our subtyping method identified two clusters with distinct ALFF patterns, which were highly consistent with the results from the discovery WHU cohort (subtype 1, $R = 0.853$, $P_{perm} < 0.001$; subtype 2, $R = 0.739$, $P_{perm} < 0.001$, Fig. 2c, Additional file 1: Fig S7).

To assess the transferability of the discovered ALFF subtypes, we applied a classifier based on ALFF analysis of the WHU cohort to assign depressed participants in the PKU cohort to one of the two subtypes (Additional file 1:Fig S8). Subsequently, we compared the predicted subtype labels generated by the classifier with those obtained from the clustering analysis of the PKU cohort. Notably, the classification accuracies consistently averaged 84%. These validation procedures collectively demonstrated the reproducibility and generalizability of the two newly identified subtypes, establishing them as robust tools for uncovering neuroimaging patterns in individuals with depression.

Validation of depression subtypes across multi-level biological hierarchies

These results reveal distinct neuroimaging patterns in the two depression subtypes, which resemble those observed in animal models. We further sought to explore the genetic susceptibility and stress mechanisms associated with these neuroimaging subtypes. Using ALFF data from the WHU cohort, we trained a classifier to categorize participants from the CMU depression cohort into these subtypes (Additional file 1: Fig S9). Subsequently, we compared ALFF features, PRS-MDD, risk gene expression, and metabolite profiles between each subtype and HC (Figs. 3, 4, and 5).

Genotype data were used to construct PRS-MDD to examine the genetic predispositions associated with the identified subtypes. Subtype 1 showed significantly elevated PRS scores at P_T of 10^{-6} ($N_{SNPs} = 27$) and 10^{-5} ($N_{SNPs} = 83$), explaining 2.7% and 2.9% of the variation, respectively, which indicates a higher genetic predisposition (Fig. 3a). By combining genome-wide association studies data with cortical expression quantitative trait loci information, we identified 179 genes significantly associated with subtype 1, with abundant expression in 11 tissues, 7 of which were brain tissues (Fig. 4a). In contrast, subtype 2 did not show significant differences in PRS scores compared to HC (Fig. 3b). For subtype 2, we identified 227 genes predominantly expressed in non-brain tissues, including the pancreas and pituitary (Fig. 4b).

Metabolite analysis identified 56 differentially expressed metabolites in subtype 1, including notably elevated levels of tryptophan and kynurenine (Fig. 5a), which are linked to 5-hydroxytryptamine (5-HT) neurotransmitter metabolism and neurodevelopmental processes. In subtype 2, 78 differential metabolites were identified (Fig. 5b). Pathway analysis indicated significant disruptions in the tricarboxylic acid cycle and alanine, aspartate, and glutamate metabolism, suggesting mitochondrial dysfunction in subtype 2 (Fig. 5c). Additionally, unique lipid abnormalities associated with oxidative stress and antioxidant systems were observed in subtype 2, including elevated levels of L-acetylcarnitine and various mono- and polyunsaturated fatty acids. These findings suggest that subtype 1 may be more influenced by genetic risk and neurodevelopmental factors, while subtype 2 may be associated with oxidative stress.

The multi-level biological findings revealed that subtype 1 exhibited a higher genetic predisposition, with enriched risk gene expression in brain regions and abnormal metabolites associated with tryptophan metabolism and neurodevelopment. In contrast, subtype 2 showed no alterations in polygenic risk scores but displayed enriched risk gene expression in non-brain tissues, along

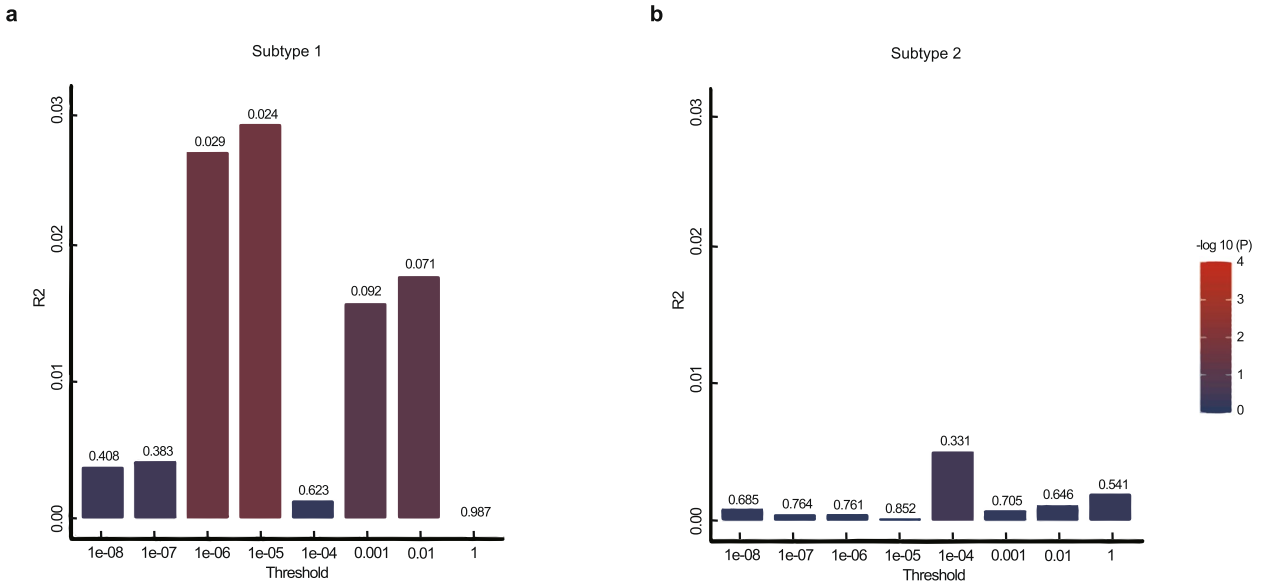

Fig. 3 Subtype-related polygenetic risk. The variance (*y*-axis) of case–control status explained by the PRS-MDD in subtype 1 (**a**) and subtype 2 (**b**). *x*-axis represents *P* value threshold, *y*-axis represents PRS model fit: R^2 (Nagelkerke's). The bars represent ten best-fit PRS scores calculated at different *P* value threshold. The significance level was set to $P < 0.05$. PRS-MDD, polygenetic risk score of major depressive disorder

with indicators of mitochondrial dysfunction and abnormalities related to oxidative stress and antioxidant systems (Additional file 1:Table S6).

Shared neuroimaging patterns across rodent models and subtypes of depression

One of the most important observations of this study was the association between the neuroimaging patterns of rodent models and patients with depression. P11 KO mice and subtype 1 had similar patterns of ALFF alterations (Fig. 6a). Likewise, CUMS and subtype 2 shared comparable ALFF patterns (Fig. 6b). Based on these parallels, we further examined co-altered ALFF patterns between the rodent models and corresponding depression subtypes.

ALFF values were extracted from regions showing significant differences, revealing substantial overlap between animal models and subtypes, particularly in subcortical and sensorimotor areas (Additional file 1:FigS1). To ensure a comprehensive understanding of overall activity level in each region, not just those voxels showing different, ALFF values were also extracted from standard atlas-defined brain regions in the subcortical and sensorimotor areas. Results indicated common alterations in most brain regions between animal models and subtypes, although not in a one-to-one correspondence (Additional file 1: Fig S10). This lack of exact alignment could be due to the smaller size of some differentially active voxel clusters, which may become less distinct when averaging ALFF values across entire brain regions.

To further validate our results, the differentially active brain regions were parcelled into three co-altered ROI based on standardized atlases: (1) subcortical ROI: including the hippocampus, amygdala, striatum, pallidum, and thalamus; (2) sensorimotor ROI: including primary motor, somatosensory, parietal cortex, visual cortex, and (3) temporal-olfactory ROI: auditory cortex, temporal cortex, and olfactory cortex. For post hoc comparison, we extracted ALFF values from ALFF values from all voxels within each ROI. Comparison with respective controls showed significantly increased ALFF in the subcortical (P11 KO mice, $T = 2.254$, $P = 0.041$; subtype 1, $T = 4.025$, $P < 0.001$) and significantly reduced ALFF in the sensorimotor (P11 KO mice, $T = -2.441$, $P = 0.029$; subtype 1 depression, $T = -8.572$, $P < 0.001$) in both P11 KO mice and subtype 1 (Fig. 6c). Contrary to P11 KO and subtype 1 depression, post hoc comparison with respective controls revealed significantly decreased ALFF in the subcortical (CUMS rats, $T = -2.758$, $P = 0.010$; subtype 2, $T = -2.560$, $P = 0.011$) and significantly elevated ALFF in the sensorimotor (CUMS rats, $T = 2.396$, $P = 0.023$; subtype 2, $T = 5.027$, $P < 0.001$) in both CUMS rats and subtype 2 (Fig. 6d). Only subtype 1 significantly increased ALFF in the temporal-olfactory ROI ($T = 2.344$, $P = 0.020$).

Subcortical-sensorimotor ALFF predicted shared anhedonia in rodent models and depression subtypes

After establishing the similarity in ALFF patterns between the rodent models and depression subtypes,

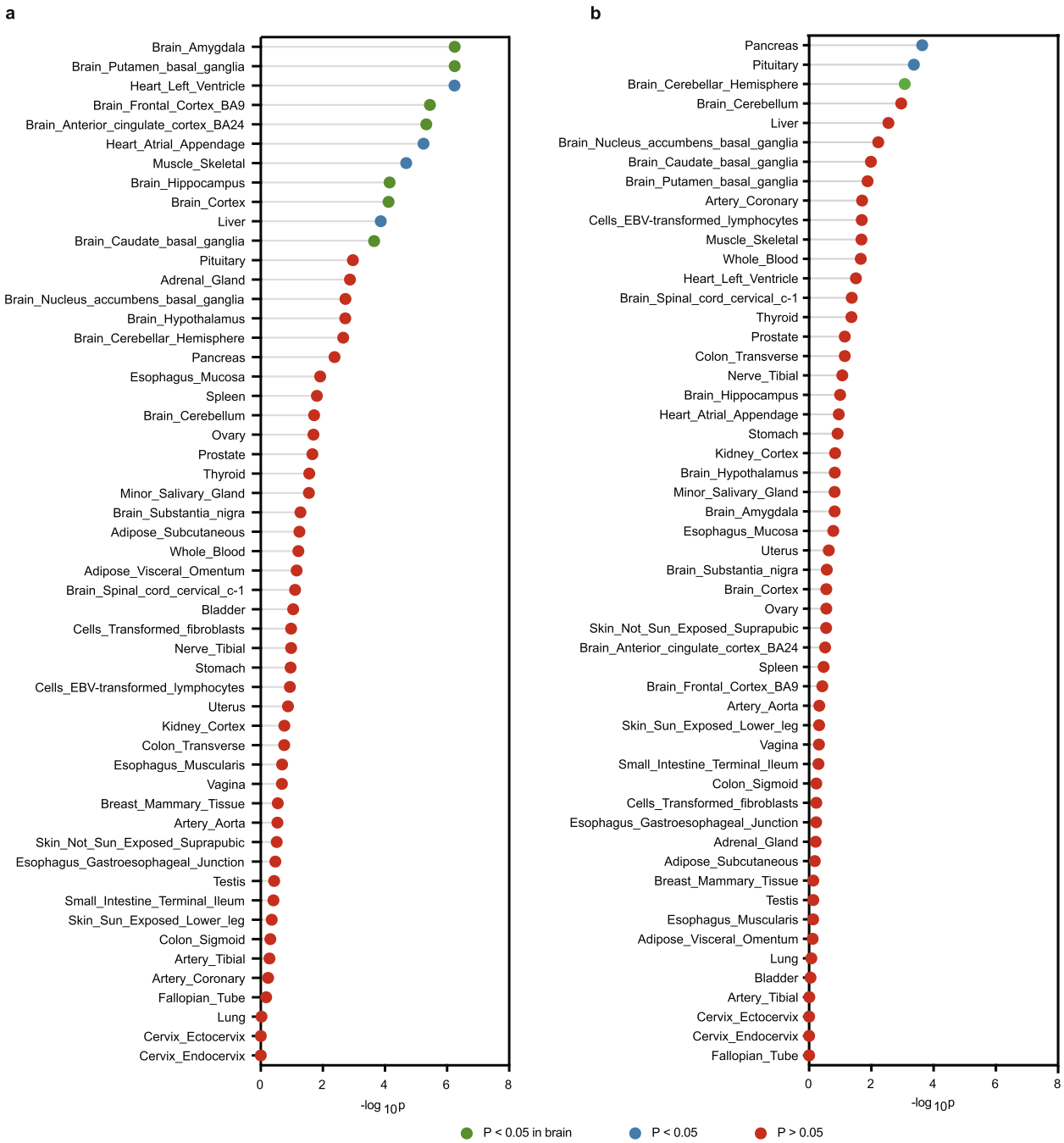

Fig. 4 Subtype-related risk gene expression. Differentially expressed risk genes across 53 tissues in **a** subtype 1 and **b** subtype 2

we investigated how these patterns related to depressive behaviors. Among the depressive behaviors examined, anhedonia was observed as a shared behavioral manifestation among both P11 KO and CUMS models (Additional file 1:Fig S11), as well as in subtype 1 and subtype 2 (Additional file 1: Table S1).

Next, we examined how the shared behavioral manifestation of anhedonia related to subcortical-sensorimotor ALFF patterns in the rodent models and depression subtypes. Using the subcortical and sensorimotor ROIs described above, we developed a stepwise linear regression model to predict anhedonia (Fig. 6e, f).

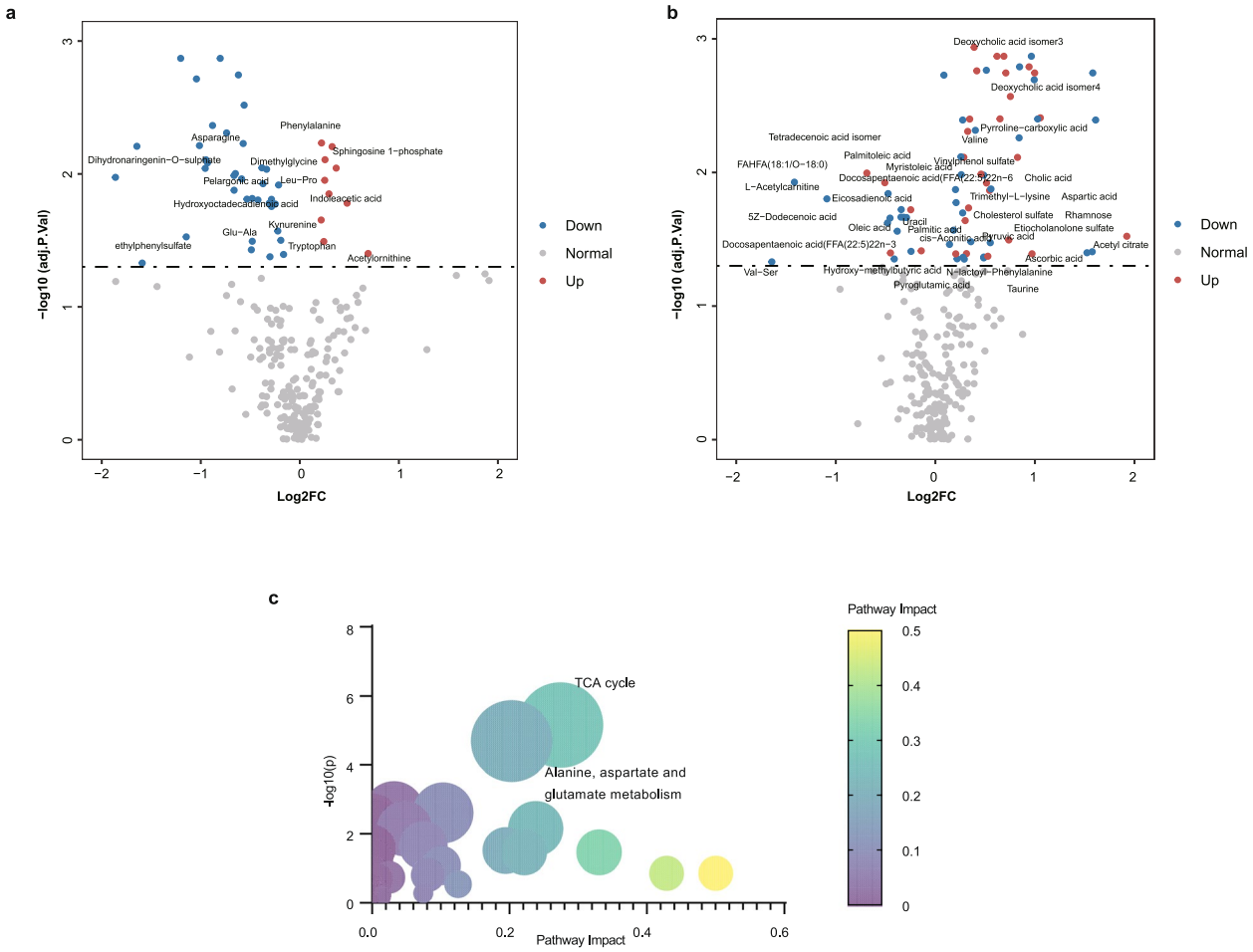

Fig. 5 Subtype-specific metabolite profiles. **a** Volcano plot illustrating metabolomic differences between subtype 1 and the HC. **b** Volcano plot illustrating metabolomic differences between subtype 2 and the HC. Red indicates upregulated metabolites compared to HC, blue represents downregulated metabolites, and gray signifies metabolites with no discernible difference. The labeled metabolites are those uniquely altered in each subtype. **c** The metabolite pathway of subtype 2. HC, healthy control; FC, fold change; TCA, tricarboxylic acid

The predicted SPT scores based on ALFF values in the subcortical (striatum) and sensorimotor (somatosensory cortex) regions showed a strong correlation with the actual measured SPT score in P11 KO mice ($R=0.8$, $P=0.003$). Similarly, the SHAPS score for subtype 1 was significantly predicted by ALFF in the striatum and somatosensory cortex ($R=0.25$, $P=0.005$). In contrast, the correlations between measured and predicted anhedonia scores based on ALFF in the striatum and somatosensory cortex were weaker but still significant for CUMS ($R=0.6$, $P=0.018$) and subtype 2 ($R=0.23$, $P=0.028$). The functional impairment of the striatum has been widely linked to anhedonia, establishing it as a key region in the reward circuitry [41, 42]. Additionally, the somatosensory cortex has been proposed as an important hub for anhedonia in depression, supported by structural and functional results [43, 44]. However, while these etiologically distinct rodent models and depression subtypes share common clinical symptoms of anhedonia, the distinct ALFF patterns suggest they may reflect different neurobiological pathways.

Discussion

Animal models and neuroimaging-derived intermediate phenotypes offer significant potential for advancing our understanding and diagnosis of neuropsychiatric disorders like depression. However, their application in unraveling the complex etiologies of depression and improving diagnostic accuracy remains underexplored. This study represents a pioneering effort in using neuroimaging as a cross-species intermediate phenotype and adopting analogous behaviors as shared symptoms to disentangle the complex etiologies of depression into genetic and stress-related mechanisms. Notably, consistent neuroimaging alterations observed in P11 KO models aligned with depression subtypes associated with a high

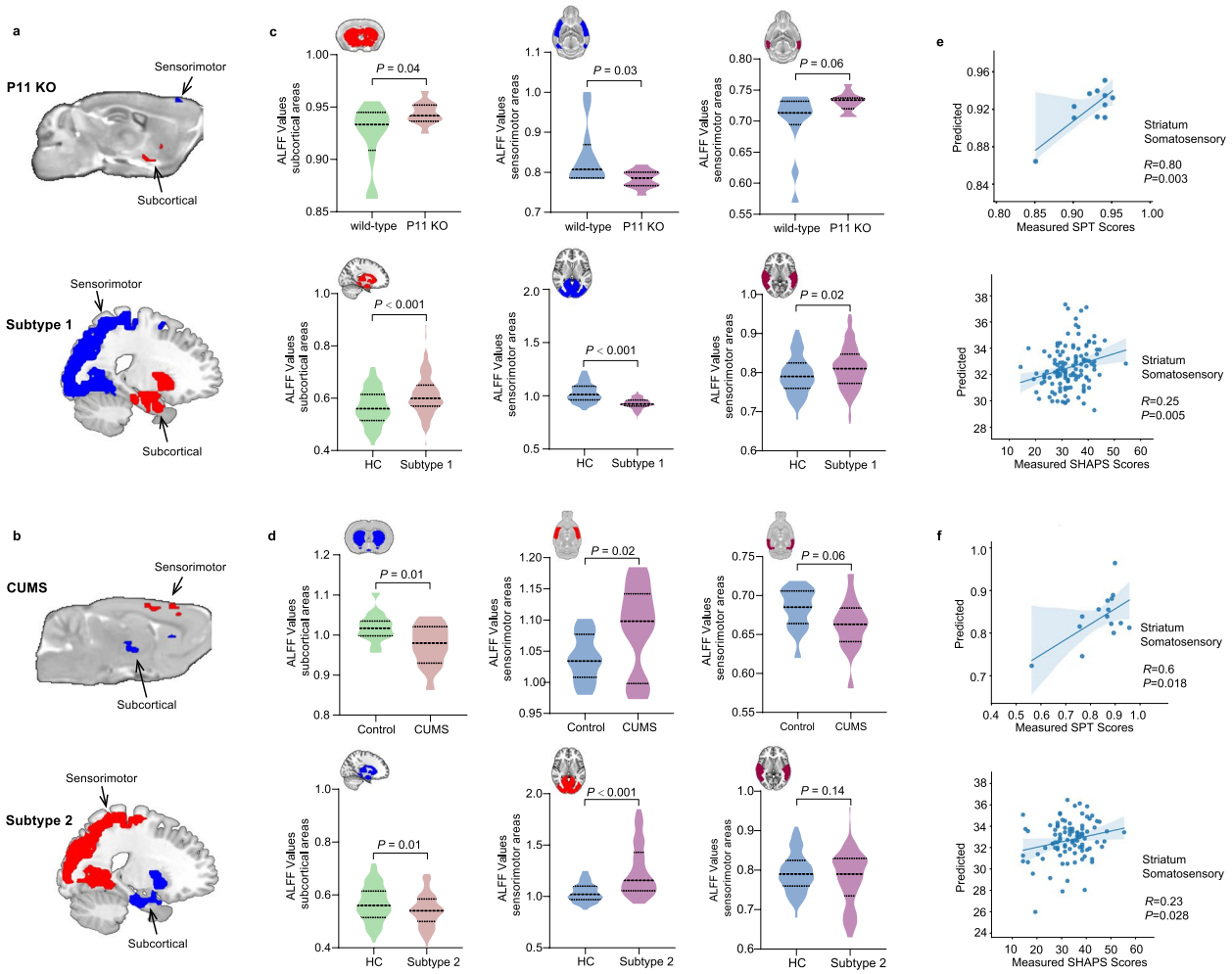

Fig. 6 Co-altered ALFF patterns in subcortical and sensorimotor predicted anhedonia. **a** Co-altered ALFF regions of the P11 KO and subtype 1. **b** Co-altered ALFF regions of the CUMS and subtype 2. **c** ALFF values showed a significant increase in subcortical and a decrease in sensorimotor regions between P11 KO and wild-type mice (top) and subtype 1 and control (bottom). Significant differences were determined using a two-tailed *t*-test with the significance value set at $P < 0.05$. **d** ALFF values showed a significant decrease in subcortical and an increase in sensorimotor between CUMS and control (top) and subtype 2 and control (bottom). Significant differences were determined using a two-tailed *t*-test with the significance value of $P < 0.05$. **e** Scatter plots showing the significant correlation between the SPT scores predicted by co-altered ROIs ALFF values and the scores observed in the P11 KO mice (top) and between the SHAPS scores predicted by co-altered ROIs ALFF values and the scores observed in subtype 1 (bottom). Shaded areas represent 95% confidence intervals. **f** Scatter plots showing the significant correlation between the SPT scores predicted by co-altered ROIs ALFF values and the scores observed in the CUMS (top) and between the SHAPS scores predicted by co-altered ROIs ALFF values and the scores observed in subtype 2 (bottom). Shaded areas represent 95% confidence intervals. ALFF, the amplitude of low-frequency fluctuation; ROI, regions of interest; P11 KO, P11 knockout; CUMS, chronic unpredicted mild stress; SPT, sucrose preference test; SHAPS, Snaith-Hamilton Pleasure Scale

polygenic risk. Conversely, CUMS models exhibited neuroimaging features consistent with stress-related depression subtypes, distinct from the alterations observed in the genetic model and subtype. Despite these differing etiologies and neuroimaging mechanisms, all models and subtypes reflected alterations in core depressive symptoms. These findings provide initial insights into the role of neuroimaging in capturing the genetic and environmental factors underlying diverse depression etiologies, bridging the translational gap across species and suggesting potential intervention targets for personalized depression therapy [45, 46].

One of the major challenges in translational research is identifying animal models that correspond to clinical populations. Our study addressed this challenge by establishing a connection between the neuroimaging characteristics of gene knockout models [47, 48] and those observed in high-risk populations for depression [49].

P11, a member of the S100 family of proteins, serves as an adapter protein that regulates 5-HT receptors 1B, 1D, and 4 [50]. Evidence from both mouse and human studies indicates that P11 is expressed in specific brain regions, including the cortex and limbic areas, which are highly relevant to depression [7, 50–53]. Notably, alterations in the mRNA and protein levels of P11 have consistently been associated with depression-like phenotypes [7]. In particular, reduced P11 levels in the nucleus accumbens are associated with depression-like behaviors, and these behaviors can be alleviated by targeted P11 gene therapy in this region [51]. Fortunately, we identified clinical subgroups that correspond to the P11 KO model. Specifically, subtype 1 exhibited abnormal metabolites associated with tryptophan and kynurenine and indoleacetic acid. These metabolic changes significantly impact 5-HT neurotransmission and ultimately affect neurodevelopment [54–56]. This finding aligns with the P11 KO model, where the deletion of P11 disrupts the 5-HTergic system. Furthermore, individuals with higher genetic risk displayed neuroimaging alterations characterized by increased activity in higher-order regions and decreased activity in primary regions [16, 49], mirroring the patterns observed in P11 KO models. These consistent patterns of altered neuroimaging activity across species indicate that enhanced subcortical and reduced sensorimotor activity may stem from genetic or neurodevelopmental processes, effectively bridging the gap between animal models and human populations as intermediate phenotypes.

In the CUMS [57] model and subtype 2, we observed a consistent pattern of decreased higher-order cortex activity and increased sensorimotor activity, contrasting with findings in the P11 KO model and subtype 1. During adolescence, the brain exhibits remarkable neuroplasticity, where early-life stress can leave lasting imprints on brain function, potentially accelerating the maturation of the primary cortex and limiting its plasticity [58, 59]. Individuals with depression who demonstrate decreased frontal-subcortical activity and increased sensorimotor activity are reported to have significant stress exposure [60, 61]. Notably, this group exhibited no significant differences in genetic risk assessments, with pronounced genetic risk gene expression found in somatic and endocrine-related tissues [16]. Our findings in subtype 2, including mitochondrial dysfunction and elevated lipids associated with oxidative stress, further underscore the impact of stressors [62–64]. These integrated results suggest that the observed neuroimaging patterns may be linked to stress-related stimuli. While our study examined two distinct rodent models, one based on genetic knockout and the other on stress conditioning, these models provide valuable insights into the endpoints along the gene-stress etiological spectrum of depression. Future research could enhance understanding by incorporating additional animal models to further explore the complex interplay between genetic and stress factors in depression.

We did not find any significant alterations in the frontal cortex of P11 KO mice or CUMS rats, but we did find significant changes in frontal regions in the depression subtypes. Differences in evolutionary processes may explain the discrepant findings in the frontal cortex across species herein [65, 66]. During mammalian evolution, the neocortex, including the frontal cortex, underwent substantial expansion, particularly in humans with larger prefrontal lobes than rodents [65]. Nevertheless, rodents and humans have a significant degree of homology [65, 67]. They exhibit evolutionarily conserved mechanisms controlling neuronal maturation, especially in subcortical regions during the early stages of development [68, 69]. The subcortical regions of both rodents and humans play a crucial role in higher-order functions such as emotion, cognition, motivation, and perception, working in conjunction with the frontal cortex [70, 71]. Our current study found that rodent models and depression subtypes shared ALFF patterns in subcortical and sensorimotor regions. This result suggests that the involvement of subcortical-sensorimotor function in depressive behaviors is conserved across species and may be fundamental and reliable biomarkers of depression.

Intriguingly, distinct patterns of subcortical-sensorimotor neuroimaging alterations, particularly in the striatum and somatosensory regions, were associated with a shared behavioral manifestation of anhedonia across different etiological rodent models and human depression cohorts. In fact, Price et al. demonstrated that depression can be categorized into subtypes based on the functional connectivity of various brain networks during positive mood induction [72]. These findings suggest that same depressive symptoms, such as anhedonia, may arise from different physiological processes. This also underscores the limited effectiveness of current clinical treatments, which often rely on symptom-based approaches without considering the diverse biological mechanisms underlying similar symptoms [73]. Additionally, our results indicate that neuroimaging serves as an effective intermediate phenotype that links underlying metabolic variations to depressive symptoms (Additional file 1: Fig.S12). Therefore, neuroimaging can serve as an intermediate phenotype to connect etiology and symptoms, providing objective biomarkers for characterizing depression subtypes [12]. This approach is crucial for developing personalized medicine tailored to individual characteristics, ultimately improving treatment outcomes for depression [74, 75].

The current study can be improved. First, we utilized young male mice to model human depression subtypes, which may limit the generalizability of our findings. Recent research indicates that the differences between male and female animals may not be as pronounced as previously believed, emphasizing the need to include both sexes in animal studies [76, 77]. While we acknowledge the common use of male participants in the field, we recognize the importance of incorporating both sexes in future research to better understand sex-related differences in neuroimaging phenotypes. Second, discrepancies in anesthesia between animal and human fMRI may introduce confounding factors, suggesting the need for awake animal scans. However, acclimating animals to restraint for awake scans involves a prolonged adaptation period and induces stress [78], necessitating careful consideration of inherent limitations in interpreting animal research. Third, certain behaviors measured in rodents, such as the SPT, might not comprehensively mirror the full spectrum of human depressive symptoms, especially nuances related to consummatory versus anticipatory anhedonia and the motivational aspects of anhedonia. While these measures capture some depressive behaviors across species, it is essential to recognize their limitations in fully representing the complexity of human depressive experiences. Additionally, incorporating more clinical depression scales could further validate our findings by capturing a broader range of depressive symptoms across diverse populations. Finally, we did not collect demographic data related to genetic and environmental factors in this cohort. Incorporating additional genetic and environmental measures in future research would help to better understand these two subtypes from a more multidimensional perspective.

Conclusions

Our study revealed a conserved role of subcortical-sensorimotor functional balance in anhedonia across both rodent models and human depression. These results support the use of subcortical-sensorimotor neuroimaging features as an effective intermediate phenotype, facilitating the translation of findings from animal models to human depression. Identifying neural subtypes based on these neuroimaging patterns offers valuable insights into potential targets for personalized therapeutic approaches. This work highlights the utility of genetic and stress animal models in unraveling the complex etiologies of depression, with promising implications for developing personalized treatment strategies.

Abbreviations

P11 KO	P11 knockout mice
CUMS	Chronic unpredictable mild stress
fMRI	Functional magnetic resonance imaging
SPT	Sucrose preference test
FST	Forced swim test
OFT	Open field test
GE EPI	Gradient-echo echo-planar imaging
ALFF	Amplitude of low-frequency fluctuation
HC	Healthy controls
WHU	The Renmin Hospital of Wuhan University
PKU	The Peking University Sixth Hospital
CMU	The First Affiliated Hospital of China Medical University
HAMD-17	17-Item Hamilton Depression Rating Scale
SHAPS	Snaith-Hamilton Pleasure Scale
FC	Functionalconnectivity
t-SNE	t-distributed Stochastic Neighbor Embedding
3D ResNet	3D Residual Networks
PRS-MDD	Polygenic Risk Scores for Major Depression Disorder
DPABI	Data Processing and Analysis of Brain Imaging
GRF	Gaussian Random Field
PT	*P*-Value thresholds
FDR	False discovery rate
ROIs	Regions of interest
MPDs	Major psychiatry disorders
5-HT	5-Hydroxytryptamine

Supplementary Information

The online version contains supplementary material available at https://doi.org/10.1186/s12916-025-03850-4.

Additional file 1. Supplemental materials, including Supplemental methods, Supplemental data Tables S1-S6, Supplemental Figures S1-S12. Tables S1. Demographic and clinical characteristics of the participant in the WHU cohort. Table S2. Demographic and clinical characteristics of the participant in the PKU and CMU cohorts. Table S3. The amplitude of low-frequency fluctuation values in brain regions showing significant differences in P11 knockout mice and wild-type mice groups.Table S4. The amplitude of low-frequency fluctuation values in brain regions, showing significant differences in CUMS and control groups. Table S5 The amplitude of low-frequency fluctuation values in brain regions, showing significant differences between subtype 1, subtype 2 and healthy control. Table S6. Distinct characteristics between subtype 1 and subtype 2. Figure S1. ALFF differences in subregions across rodent models and depression subtypes. Figure S2. Opposite ALFF patterns in animals. Figure S3. Opposite ALFF patterns of depression subtypes. Figure S4. Convergence validation of depression subtypes in FC feature. Figure S5. The t-SNE and agglomerative hierarchical clustering defined two depression neuroimaging subtypes. Figure S6. The structure of 3D Residual Networks to evaluate the classification performance. Figure S7. Validation the reproducibility of depression subtypes in an independent cohort. Figure S8. Validation transferability of depression subtypes in an independent cohort using ALFF. Figure S9. Neuroimaging pattern of subtypes in CMU. Figure S10. ALFF values extracted from standard atlas-defined brain region values in the subcortical and sensorimotor areas. Figure S11. Both P11 KO and CUMS showed anhedonia symptoms. Figure S12. Mediation model demonstrating the significant indirect effect of neuroimaging in the relationship between metabolic and symptoms.

Additional file 2. ARRIVE checklist.

Acknowledgements

Not applicable.

Authors' contributions

Conceptualization-HG, YX, DS, WZ, XZ, FW2. Validation-HG, YX, HW, RH, RL, DS, FW1, WZ, XZ, FW2. Methodology-HG, SD, JY, TZ, JW, XZ. Software-SD, JY, JW, XZ. Resources-JY, TZ, LT, JL, HW, RH, RL, YW1, ZL, MX, YH, YW2, TS, YT. Data Curation-HG, YX, JY, PZ, TZ, AC, LT, JL, HW, RH, RL, YW1, DS, ZL, MX, YH, YH, YW2, TS, YT. Formal Analysis-HG, SD, PZ, AC, LT, JL. Investigation-HG, JY, TZ, HW, RH, RL, YW1. Writing - Original Draft-HG, YX, SD, LT, JL, YW2, FW1, XZ, FW2. Writing - Review & Editing-HG, YX, SD, HW, RH, RL, DS, ZL, MX, YH, TS, FW1, FX, YT, JW, WZ, XZ,

FW2. Visualization-HG, YX, SD, PZ, AC, LT, JL, WZ, XZ. Funding acquisition-YW1, FX, WZ, XZ, FW2. Supervision-FX, JW, WZ, XZ. Project administration-FW2. All authors read and approved the final manuscript.

Funding
The study were supported by research grants from NSFC-Guangdong Joint Fund (U20A6005 to FW2), National Natural Science Foundation of China (62176129 to XZ), Jiangsu Provincial Key Research and Development Program (BE2021617 to FW2), National Natural Science Foundation of China (21921004 to FX), National Natural Science Foundation of China (82301689 to YW1), China Postdoctoral Science Foundation (2021M691643 to YW1), Hong Kong RGC Strategic Target Grant (STG1/M-501/23-N to WZ and FW2), Hong Kong Health and Medical Research Fund (10211696 to WZ), and Hong Kong Jockey Club Trust for the Hong Kong Global STEM Professorship Scheme (to WZ).

Data availability
The fMRI cohorts generated and analyzed in this study are available upon request. We also freely provide the code used to generate the data. Further information and requests for resources and reagents should be directed to and will be fulfilled by Dr. Fei Wang (fei.wang@yale.edu).

Declarations

Ethics approval and consent to participate
All procedures in these animal experiments were conducted in accordance with the guidelines of the Animal Care and Use Committee at the Wuhan Institute of Physics and Mathematics, Chinese Academy of Sciences (APM23010A). The human study was approved by the Ethics Committees of Renmin Hospital of Wuhan University (WDRY2020-K191), Peking University Sixth Hospital (2016–6), and the First Affiliated Hospital of China Medical University (2015–27-2). All human participants provided written informed consent after receiving a detailed description of the study.

Consent for publication
Written informed consent was obtained from all participants included in the study for the use of their clinical, demographic, and neuroimaging data in this publication.

Competing interests
The authors declare no competing interests.

Author details
[1]Early Intervention Unit, Department of Psychiatry, Affiliated Nanjing Brain Hospital, Nanjing Medical University, 264 Guangzhou Street, Nanjing, China. [2]School of Biomedical Engineering and Informatics, Nanjing Medical University, Nanjing, China. [3]Changzhou Medical Center, Changzhou No.2 People's Hospital, Nanjing Medical University, Changzhou, China. [4]Henan Key Laboratory of Immunology and Targeted Drugs, School of Laboratory Medicine, Xinxiang Medical University, Xinxiang, China. [5]Department of Cardiac Function, The People's Hospital of China Medical University and the People's Hospital of Liaoning Province, Shenyang, China. [6]Department of Psychiatry, Renmin Hospital of Wuhan University, Wuhan, China. [7]Taikang Center for Life and Medical Sciences, Wuhan University, Wuhan, China. [8]State Key Laboratory of Cognitive Neuroscience and Learning, Beijing Normal University, Beijing, China. [9]Beijing Key Laboratory of Brain Imaging and Connectomics, Beijing Normal University, Beijing, China. [10]IDG/McGovern Institute for Brain Research, Beijing Normal University, Beijing, China. [11]Chinese Institute for Brain Research, Beijing, China. [12]Peking University Sixth Hospital, Peking University Institute of Mental Health, NHC Key Laboratory of Mental Health (Peking University), National Clinical Research Center for Mental Disorders (Peking University Sixth Hospital), Peking University, Beijing, China. [13]Department of Psychiatry and Behavioral Sciences, Vanderbilt University Medical Center, Nashville, TN, USA. [14]Key Laboratory of Magnetic Resonance in Biological Systems, State Key Laboratory of Magnetic Resonance and Atomic and Molecular Physics, National Center for Magnetic Resonance in Wuhan, Wuhan Institute of Physics and Mathematics, Innovation Academy for Precision Measurement Science and Technology, Chinese Academy of Sciences-Wuhan National Laboratory for Optoelectronics, Wuhan, China. [15]Brain Cognition and Brain Disease Institute (BCBDI), Shenzhen Key Laboratory of Viral Vectors for Biomedicine, Shenzhen Institute of Advanced Technology, Chinese Academy of Sciences; Shenzhen-Hong Kong Institute of Brain Science-Shenzhen Fundamental Research Institutions, NMPA Key Laboratory for Research and Evaluation of Viral Vector Technology in Cell and Gene Therapy Medicinal Products, Shenzhen, Key Laboratory of Quality Control Technology for Virus-Based Therapeutics, Guangdong Provincial Medical Products Administration, Shenzhen, China. [16]Centerfor Excellence in Brain Science and Intelligence Technology, Chinese Academy of Sciences, Shanghai, China. [17]University of Chinese Academy of Sciences, Beijing, China. [18]Department of Psychiatry, Shengjing Hospital of China Medical University, Shenyang, China. [19]Songjiang Research Institute, Songjiang Hospital Affiliated to Shanghai Jiao Tong University School of Medicine, Shanghai, China. [20]Department of Health Technology and Informatics, Department of Computing, The Hong Kong Polytechnic University, Hong Kong, China. [21]Department of Mental Health, School of Public Health, Nanjing Medical University, Nanjing, China.

Received: 20 August 2024 Accepted: 8 January 2025
Published online: 23 January 2025

References

1. Kwong ASF, López-López JA, Hammerton G, Manley D, Timpson NJ, Leckie G, et al. Genetic and environmental risk factors associated with trajectories of depression symptoms from Adolescence to young adulthood. JAMA Netw Open. 2019;2(6):e196587.
2. Belzung C. Innovative drugs to treat depression: did animal models fail to be predictive or did clinical trials fail to detect effects? Neuropsychopharmacology. 2014;39(5):1041–51.
3. Griebel G, Holsboer F. Neuropeptide receptor ligands as drugs for psychiatric diseases: the end of the beginning? Nat Rev Drug Discov. 2012;11(6):462–78.
4. Chadman KK, Yang M, Crawley JN. Criteria for validating mouse models of psychiatric diseases. Am J Med Genet B Neuropsychiatr Genet. 2009;150b(1):1–11.
5. Nestler EJ, Hyman SE. Animal models of neuropsychiatric disorders. Nat Neurosci. 2010;13(10):1161–9.
6. American Psychiatric Association. Diagnostic and statistical manual of mental disorders (5th ed.). Arlington, VA: American Psychiatric Publishing; 2013.
7. Svenningsson P, Chergui K, Rachleff I, Flajolet M, Zhang X, El Yacoubi M, et al. Alterations in 5-HT1B receptor function by p11 in depression-like states. Science. 2006;311(5757):77–80.
8. Antoniuk S, Bijata M, Ponimaskin E, Wlodarczyk J. Chronic unpredictable mild stress for modeling depression in rodents: Meta-analysis of model reliability. Neurosci Biobehav Rev. 2019;99:101–16.
9. Krystal JH, State MW. Psychiatric disorders: diagnosis to therapy. Cell. 2014;157(1):201–14.
10. Beijers L, Wardenaar KJ, van Loo HM, Schoevers RA. Data-driven biological subtypes of depression: systematic review of biological approaches to depression subtyping. Mol Psychiatry. 2019;24(6):888–900.
11. Lynch CJ, Gunning FM, Liston C. Causes and consequences of diagnostic heterogeneity in depression: paths to discovering novel biological depression subtypes. Biol Psychiatry. 2020;88(1):83–94.
12. Drysdale AT, Grosenick L, Downar J, Dunlop K, Mansouri F, Meng Y, et al. Resting-state connectivity biomarkers define neurophysiological subtypes of depression. Nat Med. 2017;23(1):28–38.
13. Chang M, Edmiston EK, Womer FY, Zhou Q, Wei S, Jiang X, et al. Spontaneous low-frequency fluctuations in the neural system for emotional perception in major psychiatric disorders: amplitude similarities and differences across frequency bands. J Psychiatry Neurosci. 2019;44(2):132–41.
14. Xia M, Womer FY, Chang M, Zhu Y, Zhou Q, Edmiston EK, et al. Shared and distinct functional architectures of brain networks across psychiatric disorders. Schizophr Bull. 2019;45(2):450–63.
15. Sun X, Sun J, Lu X, Dong Q, Zhang L, Wang W, et al. Mapping neurophysiological subtypes of major depressive disorder using normative models of the functional connectome. Biol Psychiatry. 2023;94(12):936–47.
16. Chang M, Womer FY, Gong X, Chen X, Tang L, Feng R, et al. Identifying and validating subtypes within major psychiatric disorders based on frontal-posterior functional imbalance via deep learning. Mol Psychiatry. 2021;26(7):2991–3002.

17. Lou Y, Han M, Liu H, Niu Y, Liang Y, Guo J, et al. Essential roles of S100A10 in Toll-like receptor signaling and immunity to infection. Cell Mol Immunol. 2020;17(10):1053–62.
18. Strekalova T, Liu Y, Kiselev D, Khairuddin S, Chiu JLY, Lam J, et al. Chronic mild stress paradigm as a rat model of depression: facts, artifacts, and future perspectives. Psychopharmacology. 2022;239(3):663–93.
19. Yankelevitch-Yahav R, Franko M, Huly A, Doron R. The forced swim test as a model of depressive-like behavior. J Vis Exp. 2015;(97):52587.
20. Zang YF, He Y, Zhu CZ, Cao QJ, Sui MQ, Liang M, et al. Altered baseline brain activity in children with ADHD revealed by resting-state functional MRI. Brain Dev-JPN. 2007;29(2):83–91.
21. Yan CG, Wang XD, Zuo XN, Zang YF. DPABI: Data Processing & Analysis for (Resting-State) Brain Imaging. Neuroinformatics. 2016;14(3):339–51.
22. Dorr AE, Lerch JP, Spring S, Kabani N, Henkelman RM. High resolution three-dimensional brain atlas using an average magnetic resonance image of 40 adult C57Bl/6J mice. Neuroimage. 2008;42(1):60–9.
23. Barrière DA, Magalhães R, Novais A, Marques P, Selingue E, Geffroy F, et al. The SIGMA rat brain templates and atlases for multimodal MRI data analysis and visualization. Nat Commun. 2019;10(1):5699.
24. Zheng YP, Zhao JP, Phillips M, Liu JB, Cai MF, Sun SQ, et al. Validity and reliability of the Chinese Hamilton Depression Rating Scale. Br J Psychiatry. 1988;152:660–4.
25. Snaith RP, Hamilton M, Morley S, Humayan A, Hargreaves D, Trigwell P. A scale for the assessment of hedonic tone the Snaith-Hamilton Pleasure Scale. Br J Psychiatry. 1995;167(1):99–103.
26. Tzourio-Mazoyer N, Landeau B, Papathanassiou D, Crivello F, Etard O, Delcroix N, et al. Automated anatomical labeling of activations in SPM using a macroscopic anatomical parcellation of the MNI MRI single-subject brain. Neuroimage. 2002;15(1):273–89.
27. Laurens V D M , Hinton G .Visualizing Data using t-SNE. J Mach Learn Res. 2008;9(2605):2579–605.
28. Johnson SC. Hierarchical clustering schemes. Psychometrika. 1967;32(3):241–54.
29. Pedregosa F, Varoquaux G, Gramfort A, Michel V, Thirion B, Grisel O, et al. Scikit-learn: machine learning in Python. J Mach Learn Res. 2011;12:2825–30.
30. Monti S, Tamayo P, Mesirov J, Golub T. Consensus clustering: a resampling-based method for class discovery and visualization of gene expression microarray data. Mach Learn. 2003;52(1):91–118.
31. Hara K, Kataoka H, Satoh Y. Learning spatio-temporal features with 3d residual networks for action recognition. ICCVW. 2017:3154–60.
32. Han X, Jovicich J, Salat D, van der Kouwe A, Quinn B, Czanner S, et al. Reliability of MRI-derived measurements of human cerebral cortical thickness: the effects of field strength, scanner upgrade and manufacturer. Neuroimage. 2006;32(1):180–94.
33. Jovicich J, Czanner S, Greve D, Haley E, van der Kouwe A, Gollub R, et al. Reliability in multi-site structural MRI studies: effects of gradient non-linearity correction on phantom and human data. Neuroimage. 2006;30(2):436–43.
34. Takao H, Hayashi N, Ohtomo K. Effect of scanner in longitudinal studies of brain volume changes. J Magn Reson Imaging. 2011;34(2):438–44.
35. Johnson WE, Li C, Rabinovic A. Adjusting batch effects in microarray expression data using empirical Bayes methods. Biostatistics. 2007;8(1):118–27.
36. Wang Y, Lu J, Yu J, Gibbs RA, Yu F. An integrative variant analysis pipeline for accurate genotype/haplotype inference in population NGS data. Genome Res. 2013;23(5):833–42.
37. Wray NR, Ripke S, Mattheisen M, Trzaskowski M, Byrne EM, Abdellaoui A, et al. Genome-wide association analyses identify 44 risk variants and refine the genetic architecture of major depression. Nat Genet. 2018;50(5):668–81.
38. Purcell S, Neale B, Todd-Brown K, Thomas L, Ferreira MA, Bender D, et al. PLINK: a tool set for whole-genome association and population-based linkage analyses. Am J Hum Genet. 2007;81(3):559–75.
39. He X, Fuller CK, Song Y, Meng Q, Zhang B, Yang X, et al. Sherlock: detecting gene-disease associations by matching patterns of expression QTL and GWAS. Am J Hum Genet. 2013;92(5):667–80.
40. Watanabe K, Taskesen E, van Bochoven A, Posthuma D. Functional mapping and annotation of genetic associations with FUMA. Nat Commun. 2017;8(1):1826.
41. A D-A, A M. The neurobiology of anhedonia and other reward-related deficits. Trends Neurosci. 2012;35(1):68–77.
42. Phillips ML, Chase HW, Sheline YI, Etkin A, Almeida JR, Deckersbach T, et al. Identifying predictors, moderators, and mediators of antidepressant response in major depressive disorder: neuroimaging approaches. Am J Psychiat. 2015;172(2):124–38.
43. Zhu X, Ward J, Cullen B, Lyall DM, Strawbridge RJ, Lyall LM, et al. Phenotypic and genetic associations between anhedonia and brain structure in UK Biobank. Transl Psychiatry. 2021;11(1):395.
44. Wang W, Zhou E, Nie Z, Deng Z, Gong Q, Ma S, et al. Exploring mechanisms of anhedonia in depression through neuroimaging and data-driven approaches. J Affect Disord. 2024;363:409–19.
45. Matthews PM, Honey GD, Bullmore ET. Applications of fMRI in translational medicine and clinical practice. Nat Rev Neurosci. 2006;7(9):732–44.
46. Xiao Y, Womer FY, Dong S, Zhu R, Zhang R, Yang J, et al. A neuroimaging-based precision medicine framework for depression. Asian J Psychiatr. 2024;91:103803.
47. Li Q, Zhao W, Liu S, Zhao Y, Pan W, Wang X, et al. Partial resistance to citalopram in a Wistar-Kyoto rat model of depression: An evaluation using resting-state functional MRI and graph analysis. J Psychiatr Res. 2022;151:242–51.
48. Bennett MR. Synapse regression in depression: the role of 5-HT receptors in modulating NMDA receptor function and synaptic plasticity. Aust N Z J Psychiatry. 2010;44(4):301–8.
49. Cui L, Gong X, Tang Y, Kong L, Chang M, Geng H, et al. Relationship between the LHPP Gene Polymorphism and Resting-State Brain Activity in Major Depressive Disorder. Neural Plast. 2016;2016:9162590.
50. Svenningsson P, Kim Y, Warner-Schmidt J, Oh YS, Greengard P. p11 and its role in depression and therapeutic responses to antidepressants. Nat Rev Neurosci. 2013;14(10):673–80.
51. Alexander B, Warner-Schmidt J, Eriksson T, Tamminga C, Arango-Lievano M, Ghose S et al. Reversal of depressed behaviors in mice by p11 gene therapy in the nucleus accumbens. Sci Transl Med. 2010;2(54):54ra76.
52. Schmidt EF, Warner-Schmidt JL, Otopalik BG, Pickett SB, Greengard P, Heintz N. Identification of the cortical neurons that mediate antidepressant responses. Cell. 2012;149(5):1152–63.
53. Anisman H, Du L, Palkovits M, Faludi G, Kovacs GG, Szontagh-Kishazi P, et al. Serotonin receptor subtype and p11 mRNA expression in stress-relevant brain regions of suicide and control subjects. J Psychiatry Neurosci. 2008;33(2):131–41.
54. Huang X, Feng Z, Cheng HW. Perspective: Gestational Tryptophan Fluctuation Altering Neuroembryogenesis and Psychosocial Development. Cells. 2022;11(8):1270.
55. Bonnin A, Goeden N, Chen K, Wilson ML, King J, Shih JC, et al. A transient placental source of serotonin for the fetal forebrain. Nature. 2011;472(7343):347–50.
56. Murakami Y, Imamura Y, Kasahara Y, Yoshida C, Momono Y, Fang K, et al. Maternal inflammation with elevated kynurenine metabolites is related to the risk of abnormal brain development and behavioral changes in autism spectrum disorder. Cells. 2023;12(7):1087.
57. Huang P, Dong Z, Huang W, Zhou C, Zhong W, Hu P, et al. Voluntary wheel running ameliorates depression-like behaviors and brain blood oxygen level-dependent signals in chronic unpredictable mild stress mice. Behav Brain Res. 2017;330:17–24.
58. Tooley UA, Bassett DS, Mackey AP. Environmental influences on the pace of brain development. Nat Rev Neurosci. 2021;22(6):372–84.
59. Sydnor VJ, Larsen B, Seidlitz J, Adebimpe A, Alexander-Bloch AF, Bassett DS, et al. Intrinsic activity development unfolds along a sensorimotor-association cortical axis in youth. Nat Neurosci. 2023;26(4):638–49.
60. Nagy SA, Kürtös Z, Németh N, Perlaki G, Csernela E, Lakner FE, et al. Childhood maltreatment results in altered deactivation of reward processing circuits in depressed patients: A functional magnetic resonance imaging study of a facial emotion recognition task. Neurobiol Stress. 2021;15:100399.
61. Ming Q, Zhong X, Zhang X, Pu W, Dong D, Jiang Y, et al. State-independent and dependent neural responses to psychosocial stress in current and remitted depression. Am J Psychiat. 2017;174(10):971–9.
62. Quiles JL, Barja G, Battino M, Mataix J, Solfrizzi V. Role of olive oil and monounsaturated fatty acids in mitochondrial oxidative stress and aging. Nutrition reviews. 2006;64(suppl_4):S31-S39.

63. Traina G. The neurobiology of acetyl-L-carnitine. Front Biosci Landmrk. 2016;21(7):1314–29.
64. Münzel T, Daiber A. Environmental stressors and their impact on health and disease with focus on oxidative stress. Antioxid Redox Signal. 2018;28(9):735–40.
65. Chin R, Chang SWC, Holmes AJ. Beyond cortex: The evolution of the human brain. Psychol Rev. 2023;130(2):285–307.
66. Cheng Y, Ma Z, Kim BH, Wu W, Cayting P, Boyle AP, et al. Principles of regulatory information conservation between mouse and human. Nature. 2014;515(7527):371–5.
67. Hodge RD, Bakken TE, Miller JA, Smith KA, Barkan ER, Graybuck LT, et al. Conserved cell types with divergent features in human versus mouse cortex. Nature. 2019;573(7772):61–8.
68. Yuan W, Ma S, Brown JR, Kim K, Murek V, Trastulla L, et al. Temporally divergent regulatory mechanisms govern neuronal diversification and maturation in the mouse and marmoset neocortex. Nat Neurosci. 2022;25(8):1049–58.
69. Shi Y, Wang M, Mi D, Lu T, Wang B, Dong H et al. Mouse and human share conserved transcriptional programs for interneuron development. Science. 2021; 374(6573):eabj6641.
70. Chen P, Hong W. Neural circuit mechanisms of social behavior. Neuron. 2018;98(1):16–30.
71. Salzman CD, Fusi S. Emotion, cognition, and mental state representation in amygdala and prefrontal cortex. Annu Rev Neurosci. 2010;33:173–202.
72. Price RB, Lane S, Gates K, Kraynak TE, Horner MS, Thase ME, et al. Parsing heterogeneity in the brain connectivity of depressed and healthy adults during positive mood. Biol Psychiatry. 2017;81(4):347–57.
73. Stein DJ, Shoptaw SJ, Vigo DV, Lund C, Cuijpers P, Bantjes J, et al. Psychiatric diagnosis and treatment in the 21st century: paradigm shifts versus incremental integration. World Psychiatry. 2022;21(3):393–414.
74. Nestor SM, Blumberger DM. Mapping symptom clusters to circuits: toward personalizing tms targets to improve treatment outcomes in depression. Am J Psychiatry. 2020;177(5):373–5.
75. Tozzi L, Zhang X, Pines A, Olmsted AM, Zhai ES, Anene ET, et al. Personalized brain circuit scores identify clinically distinct biotypes in depression and anxiety. Nat Med. 2024;30(7):2076–87.
76. Kaluve AM, Le JT, Graham BM. Female rodents are not more variable than male rodents: A meta-analysis of preclinical studies of fear and anxiety. Neurosci Biobehav Rev. 2022;143:104962.
77. Shansky RM. Are hormones a "female problem" for animal research? Science. 2019;364(6443):825–6.
78. Behroozi M, Helluy X, Ströckens F, Gao M, Pusch R, Tabrik S, et al. Event-related functional MRI of awake behaving pigeons at 7T. Nat Commun. 2020;11(1):4715.

Publisher's Note